Available online at www.sciencedirect.com

SCIENCE DIRECT®

Biochimica et Biophysica Acta 1664 (2004) 241–256

BIOCHIMICA ET BIOPHYSICA ACTA
BBA

www.bba-direct.com

Direct observation and characterization of DMPC/DHPC aggregates under conditions relevant for biological solution NMR

Lorens van Dam*, Göran Karlsson, Katarina Edwards*

Department of Physical Chemistry, Biomedical Center (BMC), Uppsala University, Box 579, S-751 23 Uppsala, Sweden

Received 26 March 2004; received in revised form 8 June 2004; accepted 15 June 2004
Available online 4 July 2004

Abstract

We have used cryo-transmission electron microscopy (cryo-TEM) for inspection of aggregates formed by dimyristoylphosphatidylcholine (DMPC) and dihexanoylphosphatidylcholine (DHPC) in aqueous solution at total phospholipid concentrations $c_L \leq 5\%$ and DMPC/DHPC ratios $q \leq 4.0$. In combination with ocular inspections, we are able to sketch out this part of phase-diagram at $T = 14-80$ °C. The temperature and the ratio q are the dominating variables for changing sample morphology, while c_L to a lesser extent affects the aggregate structure. At $q = 0.5$, small, possibly disc-shaped, aggregates with a diameter of ~ 6 nm are formed. At higher q-values, distorted discoidal micelles that tend to short cylindrical micelles are observed. The more well-shaped discs have a diameter of around 20 nm. Upon increasing q or the temperature, long slightly flattened cylindrical micelles that eventually branch are formed. A holey lamellar phase finally appears upon further elevation of q or temperature. The implications for biological NMR work are two. First, discs prepared as membrane mimics are frequently much smaller than predicted by current ''ideal bicelle'' models. Second, the $q \approx 3$ preparations used for aligning water-soluble biomolecules in magnetic fields consist of perforated lamellar sheets. Furthermore, the discovered sequence of morphological transitions may have important implications for the development of bicelle-based membrane protein crystallization methods.

Keywords: Bicelle; Discoidal micelle; DMPC/DHPC; Model membrane; Membrane protein structure; Magnetically aligned NMR solvent

1. Introduction

Aggregates composed of the short-chain phospholipid DHPC (dihexanoylphosphatidylcholine, dicaproylphosphatidylcholine, di-C_6 lecithin) and the long-chain phospholipid DMPC (dimyristoylphosphatidylcholine, di-C_{14} lecithin) have found use in the structural elucidation of biological macromolecules (polynucleic acids, polypeptides and proteins) by NMR. The function of the aggregates is twofold. For one, DMPC/DHPC mixtures with a relatively high amount of DHPC, typically DHPC/DMPC = 2:1, are believed to form discoidal structures. The discs, often referred to as ''bicelles'', have been proposed to consist of a circular center made of DMPC in a bilayer, or lamellar, arrangement, surrounded by a rim of DHPC [1]. This model, originally proposed in bile salt/lecithin mixtures [2,3], is known as the ''ideal bicelle'' model [4]. Such discs present a better alternative to globular micelles as membrane mimics for the extraction of biologically relevant membrane protein (polypeptide) structures by NMR [5–7]. A second use of DMPC/DHPC mixtures is through the ability of the aggregates formed at higher amounts of DMPC, typically DHPC/DMPC ≈ 1:3, to align in NMR magnetic fields. In this way, a slightly ordered solvent is obtained for the biomolecules, which gives rise to unaveraged, or residual, internuclear dipolar couplings that aid in the structural elucidation of the biomolecule dissolved [8–10]. These aggregates have also been believed to be disc-shaped [4,11,12], although recent experimental evidence seems to indicate otherwise [13–15]. Recently, DMPC/DHPC mixtures have also successfully been used in the crystallization of a membrane protein for X-ray analysis [16] (see also the recent review by Caffrey [17]), and in the capillary electrophoresis of amphiphilic drug molecules [18].

The water (i.e. buffer)-dissolved mixtures of DHPC and DMPC are typically characterized by c_L, the total weight of phospholipids per weight of solvent, and q, the molar ratio of

* Corresponding authors. Tel.: +46-18-471-3668; fax: +46-18-471-3654.
E-mail addresses: lorens.van.dam@fki.uu.se (L. van Dam), katarina.edwards@fki.uu.se (K. Edwards*).

0005-2736/$ - see front matter © 2004 Elsevier B.V. All rights reserved.
doi:10.1016/j.bbamem.2004.06.005

long-chain to short-chain phospholipid (q=[DMPC]/[DHPC]). In terms of these parameters, the small (non-aligning) DMPC/DHPC discs used as model membranes in NMR form at low values of q, typically $q = 0.5–1$, and a phospholipid concentration of around $c_L = 5–15\%$ [7]. The magnetically alignable larger aggregates are typically prepared at $3\% < c_L < 5\%$ and $q = 3.0–3.5$ [19]. According to the ideal disc model, the ratio q effectively and straightforwardly controls the size of the bicelle discs by specifying how much short-chain phospholipid is available for the formation of the rim of the disc. c_L, then, controls the number of discs that are formed. However, it has been shown that there are several other parameters that come into play when preparing these DMPC/DHPC aggregates. One of these is the monomer solubility of the short-chain phospholipid (DHPC), an effect that alters the DMPC/DHPC ratio of the aggregates formed. Another complication is the different effective head group areas occupied by DHPC in the rim and DMPC in the bilayer. These effects have been invoked in the "refined ideal bicelle model" in order to explain bicelle disc size as found by light-scattering experiments [20]. Furthermore, there are indications that the NaCl concentration of the buffer has an effect on the DMPC/DHPC systems [19], which is remarkable considering the zwitterionic identity of the phosphatidylcholine head group.

Despite the popularity of DMPC/DHPC aggregates for use in biological high-resolution NMR, and the numerous investigations of the system, there is still no solid evidence of the existence of the discoidal micelles, and it has recently been doubted that large distinct bicelle discs do exist at all under the conditions (temperatures 25–38 °C, pH 6–8) typically used [13–15,21]. Several attempts at characterizing the phase-behavior of water-dissolved DMPC/DHPC mixtures have been made, and several suggestions are to be found in the current literature [22–24]. The structures of the aggregates formed have been characterized through the interpretation of a variety of spectroscopic data, mainly (and not surprisingly) NMR [11,19,22] but also light- [20] and neutron-scattering [14,24,25], as well as fluorescence spectroscopy [15,20]. Some electron micrographs, obtained after negative staining of the samples, have also been published in the literature [20,26], but the technique renders it difficult to assess whether the pictures give a true representation of the sample morphology.

In the present study, we investigate the phase-behavior and aggregate structure of DMPC/DHPC mixtures in "physiological" buffer (20 mM HEPES, pH 7.4, 150 mM NaCl) under conditions covering those used in biological solution NMR, $1\% \le c_L \le 5\%$ and $0.5 \le q \le 4.0$. This range covers both the isotropically tumbling small bicelle discs used as membrane mimics, and the larger aggregates used to achieve magnetically aligned solvents for water-dissolved biomolecules. We use cryogenic transmission electron microscopy (cryo-TEM) in combination with ocular inspection as our main method, and supplement this technique with dynamic light scattering (DLS). The cryo-TEM technique is ideally suited for direct observation of aggregates in the size-range of 10–500 nm in dilute water-based solutions, and offers a reliable means to determine sample morphology at the aggregate level [27]. Detailed information on the average size of the aggregates is collected more suitably from DLS. We also use fluorescence spectroscopy in order to address the question of DHPC monomer solubility as a function of temperature.

2. Materials and methods

2.1. Preparation of samples

Dihexanoylphosphatidylcholine (DHPC) and dimyristoylphosphatidylcholine (DMPC) were purchased as dry powders from Avanti Polar Lipids (Alabaster, AL, USA) and used as received. Separate 100 mM stock solutions of DHPC and DMPC were prepared by carefully weighing in the appropriate amounts of chemicals and pre-prepared buffer. DHPC is hygroscopic, and therefore the weighing was performed rapidly from a freshly opened can. DHPC readily dissolves in water, while DMPC does not. The DMPC stock was therefore vigorously vortexed and heated to about 40 °C to get a homogeneous dispersion, and always vortexed just before taking out aliquots.

DMPC/DHPC samples were prepared by adding the appropriate volume of DHPC from the stock solution to a DMPC solution prepared from mixing the appropriate volume of the DMPC stock solution with the appropriate volume of additional buffer. The amounts were calculated from the relations: $c_L = \{m(\text{DHPC}) + m(\text{DMPC})\}/m(\text{buffer})$ and q=[DMPC]/[DHPC]. The amount of buffer was determined by volume, using a density of 1.0 g/ml. The solutions of DMPC/DHPC were heated to 40 °C and vortexed, then cooled to 4 °C and vortexed again, and this cycle was repeated five or more times. All stocks and samples were prepared in 20 mM HEPES buffer at pH = 7.4, with 150 mM NaCl added, unless otherwise stated. In order to prevent bacterial growth, the buffer also contained 0.01% NaN_3. Samples were stored in freezer between measurements, and were always vortexed after thawing.

2.2. Cryo-TEM

Electron microscopy was performed using a Zeiss EM 902A Transmission Electron Microscope (LEO Electron Microscopy, Oberkochen, Germany) operating at 80 kV in zero-loss bright-field mode. Digital images were recorded using a BioVision Pro-SM Slow Scan CCD camera (Proscan, Scheuring, Germany), giving a digital resolution corresponding to a pixel size of 1.6×1.6 nm at the magnification most frequently used ($10^5 \times$). The sample preparation procedure has recently been reviewed [27], and consists in short of the following steps: (1) The solution to be investigated is left in a thermostated chamber at (close to)

100% relative humidity. (2) Typically 1 μl of the solution is taken out with a pipette and deposited on a Cu grid covered by a holey polymer film. (3) Excess solution is blotted away, and the grid is then immediately dropped into liquid ethane at −165 °C. (4) The grid is mounted into the microscopy specimen holder and then transferred in a liquid nitrogen cooled transfer unit to the microscope.

2.3. Dynamic laser-light scattering

Light from an Ar-ion laser (Coherent, Palo Alto, CA) emitting at 488 or 496 nm was passed through vertical polarizers and then directed into a sample emerged in a large thermostated decaline bath. The scattered light was again passed through vertical polarizers, to detect the polarized scattered light. The detector system included a ITT FW 130 photomultiplier (Fort Wayne, IN), an ALV-PM-PD amplifier-discriminator (Langen, Germany), and an ALV-5000 autocorrelator built into a computer. The intensity–intensity autocorrelation function was measured (collection time 3 min) and the (logarithmic) electric field autocorrelation relaxation time distribution $w(\tau)$ extracted through inverse Laplace transformation and nonlinear least-square fitting, using the constrained regularization routine REPES [28,29]. The autocorrelation relaxation rate $\Gamma=\tau^{-1}$ is related to the diffusion coefficient D of the particles via:

$$D=\frac{\Gamma}{Q^2} \tag{1}$$

with Q the scattering vector $Q=4\pi n_s\sin(\theta/2)/\lambda$, where n_s is the solvent refractive index ($n_s=1.33$ for water), θ is the scattering angle ($\theta=90°$ in our measurements) and λ is the wavelength of the incoming light ($\lambda=488$ or 496 nm in our case). When varying θ from 50° to 130° (in steps of 20°, i.e., five points in total), we found a linear relation between Γ and Q^2 ($R^2=0.9967$), with a negligible intercept. This proves that Eq. (1) was valid for the sample, which was prepared at $c_L=2\%$ and $q=0.5$, and measured at 30 °C. We assume that Eq. (1) holds also for our other samples, and henceforth measure at only one scattering angle, $\theta=90°$.

At high dilution, the diffusion coefficient of small particles may be approximated by [30]:

$$D=D_0(1+k_Dc_L) \tag{2}$$

with k_D the hydrodynamic virial coefficient characterizing the thermodynamic and hydrodynamic interactions between the particles. D_0 is the diffusion coefficient at infinite dilution, i.e., in the absence of any interparticle interaction, and is related to the particle hydrodynamic radius via the Stokes–Einstein relation:

$$R_h=\frac{k_BT}{6\pi\eta D_0} \tag{3}$$

with R_h the hydrodynamic radius of the "corresponding sphere" in the case of nonspherical particles, k_B the Boltzmann constant, and η the viscosity of the solvent. We have used the viscosity of water at the specified temperature in all our calculations.

For a disc-shaped object, the relation between the disc radius r' and the hydrodynamic radius (of the corresponding sphere) is [3]:

$$R_h=\frac{3}{2}r'\left\{\sqrt{1+\left(\frac{t}{2r'}\right)^2}+\frac{2r'}{t}\ln\left[\frac{t}{2r'}+\sqrt{1+\left(\frac{t}{2r'}\right)^2}\right]-\frac{t}{2r'}\right\}^{-1} \tag{4}$$

Here t is the thickness of the phospholipid bilayer (see Fig. 1), which for DMPC is 3.7–4.4 nm, the latter value including hydrational water [31]. In the absence of accurate knowledge on the hydrodynamic properties of the hydration shell, we choose to use an intermediate value of $t=4.0$ nm for the DMPC bilayer thickness. Using $t=5.0$ nm (as in Ref. [20]) gives a 0.3 nm smaller value for r' at the same R_h (for $R_h>3$ nm).

2.4. Fluorescence spectroscopy

The fluorescent probe all-*trans*-1,6-diphenyl-1,3,5-hexatriene (DPH) was used to detect the formation of DHPC micelles [32,33]. Twenty microliters of a 0.4 mM DPH solution in methanol was added to vials, which were left open for 1 h at room temperature to allow for the methanol to evaporate. Buffer solution and subsequently a 100 mM DHPC solution (in buffer) were added in appropriate amounts to yield 1.50-ml solutions of DHPC in buffer at varying concentrations. A SPEX fluorolog 1650 0.22-m double-spectrometer (SPEX Industries, Edison, NJ) was used with all slits set to 1.0 mm, the excitation wavelength at 352 nm and the emission wavelength scanned from 413 to 443 nm. The fluorescence intensity was taken at 428 nm, which is where DPH showed maximum emission. Samples were kept in a water bath at the temperature at which measurements were done for at least half an hour prior to measurements. The sample under investigation was swiftly transferred from the water bath to a preheated/precooled kyvette (1.0 × 1.0-cm quarts) and put into the thermostated fluorolog, where it was kept to stabilize for 1–3 min, or longer time for temperatures far from room temperature, before measuring.

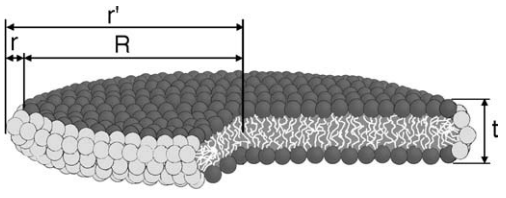

Fig. 1. A schematic picture of an ideal disc with the notation used. Black head groups represent DMPC (the long-chain phospholipid); light-grey head groups represent DHPC (the short-chain phospholipid).

2.5. Ideal disc models

In interpreting our results, we shall make use of the "ideal disc" model that has been presented by Vold and Prosser [4] as a basis. The model assumes that the long-chain phospholipid (DMPC) is exclusively situated in a bilayered fashion making up the center of the disc. The short-chain phospholipid (DHPC), then, exclusively makes up the rim of the disc. A model of the ideal disc is presented in Fig. 1. From purely geometric considerations, the relative areas of the center and the rim parts of the disc, A_{center} and A_{rim}, respectively, may be connected to the relative concentrations of the two phospholipids through [4]:

$$q = \frac{[\text{DMPC}]}{[\text{DHPC}]} = \frac{A_{\text{center}}}{A_{\text{rim}}} = \frac{R^2}{(\pi R + 2r)r} \tag{5}$$

Here r is the radius of the rim, and R is the radius of the center (bilayer) part of the disc (see Fig. 1). A value of $r = 2.0$ nm has been suggested for DMPC/DHPC discs [4], which should be a reasonable estimate considering the thickness of the DMPC bilayer (~ 4 nm [31]) and the DHPC micellar size [35].

Eq. (5), however, assumes that the phospholipids in the bilayer and in the rim occupy the same head group areas. Furthermore, the concentration of free (monomeric) DHPC, $[\text{DHPC}]_{\text{free}}$, has not been considered in this model. A refined ideal disc model, where these two effects are invoked, reads [20]:

$$q_{\text{eff}} = \frac{[\text{DMPC}]}{[\text{DHPC}]_{\text{tot}} - [\text{DHPC}]_{\text{free}}} = \frac{[\text{DMPC}]}{[\text{DHPC}]_{\text{bound}}} = k^{-1}\frac{A_{\text{center}}}{A_{\text{rim}}} = \frac{R^2}{k(\pi R + 2r)r} \tag{6}$$

with $[\text{DHPC}]_{\text{tot}}$ the total DHPC concentration, and $[\text{DHPC}]_{\text{bound}}$ the concentration of DHPC forming the rims of the discs. k is a measure of the relative head group areas, a_{head}, of the bilayer and rim-forming constituents:

$$k = \frac{a_{\text{head}}(\text{DMPC})}{a_{\text{head}}(\text{DHPC})} \tag{7}$$

Values of the head group areas may be found in the literature. For DMPC in a bilayer arrangement, a head group area of 0.60 nm^2 has been found [31]. Head group areas of 0.66 nm^2 [34] and 1.02 nm^2 [35] have been derived for pure micellar DHPC. The former value for the DHPC head group area (0.66 nm^2) is very similar to the head group area of DMPC, thus rendering $k \approx 1$. The latter value for the head group of DHPC (1.02 nm^2), leads to $k = 0.6$, which is the value used by Glover et al. [20]. We will use both these values ($k = 1$ and $k = 0.6$) in our calculations to follow.

For the purpose of calculating the disc size, Eq. (6) may be more conveniently recast as:

$$R = \frac{kq_{\text{eff}}r}{2}\left(\pi + \sqrt{\pi^2 + \frac{8}{kq_{\text{eff}}}}\right) \tag{8}$$

3. Results

3.1. Temperature dependence of the cmc of DHPC

It has been suggested in recent studies that the temperature-dependent phase-behavior of DMPC/DHPC mixtures is in part explained by the temperature dependence of the solubility of DHPC [19,20]. In order to elucidate this, we performed measurements of the critical micelle concentration (cmc) of DHPC as a function of temperature. The cmc was detected using the fluorescent probe DPH (all-*trans*-1,6-diphenyl-1,3,5-hexatriene), which shows a large increase in fluorescence when incorporated into a micellar structure (see Materials and methods). The results displayed in Fig. 2 show that the cmc of DHPC is not affected by temperature within the accuracy of the experiment (< 1 mM), but stays at 14–15 mM throughout the temperature interval 15–45 °C. (The overall increase in fluorescence as the temperature is elevated is due to the properties of DPH itself [33].) The determined cmc is in good agreement with values from the literature at 25–30 °C [34,36]. This strongly indicates that the DHPC monomer solubility is insensitive to temperature changes in the interval from 15 to 45 °C. It should be pointed out that this only means that the DHPC molecules do not change in terms of their hydrophilicity with temperature. The actual $[\text{DHPC}]_{\text{free}}$ in a given DMPC/DHPC system may still depend on temperature in an indirect fashion via changes in the alternative DHPC environments (i.e., in the DMPC/DHPC aggregate structure).

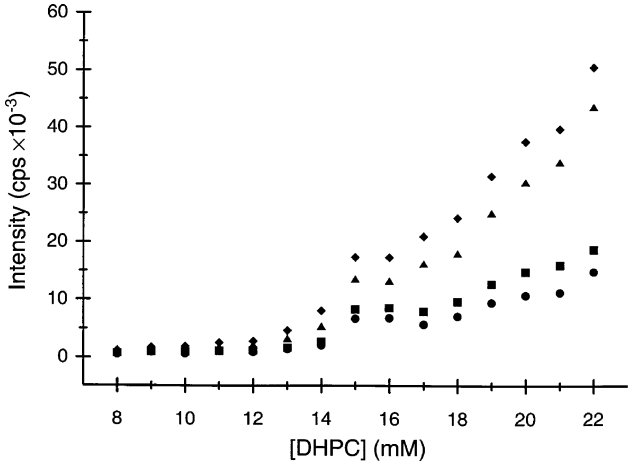

Fig. 2. Fluorescent intensity (cps) of DPH as function of DHPC concentration at 15 °C (circles), 24 °C (squares), 35 °C (triangles) and 45 °C (diamonds).

3.2. Ocular observations of DMPC/DHPC phase transitions

Samples of compositions $c_L = 1.0\%$, 2.0%, 3.0% and 5.0% with $q = 1.0$, 2.0, 3.0, and 4.0 were prepared as described in Materials and methods and put in a thermostated water bath. The temperature of the bath was increased slowly from 14 to 80 °C in steps of 1–2 °C, and the 16 samples were characterized by their macroscopic turbidity and viscosity. The general sample behavior included a clear and fluid solution at low temperature, an increased viscosity at higher temperature, and finally, as temperature was further elevated, an onset and subsequent increase in sample turbidity accompanied by a decrease in viscosity. All macroscopic transitions were reversible and occurred at approximately the same temperature in both directions.

The transition temperatures for the samples are collected in Table 1. The transition from a water-like to a viscous sample fluidity was abrupt, i.e., occurred over a narrow (1–2 °C) temperature interval, while the transition from a clear to a turbid appearance was gradual over a larger temperature span (typically 2–5 °C). Therefore, the temperature of the first transition, T_{fv}, is better determined than that of the second, T_{ct}, which should be taken as approximate. The drop in viscosity accompanying the onset of turbidity was also gradual, and the two effects appeared to be coupled. This behavior of the viscosity (abrupt increased and gradual decrease as temperature is elevated) is in line with the observations of Struppe and Vold [37]. Table 1 also reports the temperature interval over which the sample was viscous.

From the data presented in Table 1, several trends can be observed:

(i) At a given c_L, T_{ct} shifts downwards with increasing values of q. (A similar trend may be inferred for T_{fv}, although the data points are too few to be definite about this.)
(ii) At a given q, T_{ct} shifts upwards with increasing values of c_L for $q \leq 3$. (A similar trend may be seen for T_{fv} at $q = 2$.)
(iii) The temperature span over which the viscous phase exists increases with increasing c_L and with decreasing q (for samples where the viscous phase is at all observed).

Below $c_L \approx 2\%$ the viscous phase was not observed at all, which could be an effect of the crudeness of the method used to detect it. The viscosity was far greater for high c_L samples than that for low c_L samples, in line with previous observations [37], and it is plausible that a small viscosity increase at low c_L was simply not detected. At the higher values of q and c_L, e.g., the samples $c_L = 5.0\%$, $2.0 \leq q \leq 4.0$, the viscosity was so high that the fluidity tended to zero, and the solution may thus better be termed a gel (the solution did not flow when the sample was turned upside down).

There are limiting values towards the lower and higher ends of q, beyond which the viscous phase never exists. At the higher end of q, it is seen from Table 1 that the temperature of viscosity onset and the turbidity onset close up and eventually coincide with the main transition temperature of DMPC ($T_m = 24$ °C). These samples immediately turned very turbid when heated to 24 °C, and retained the viscosity of water. Towards the lower end of q, transition temperatures become dramatically higher. It is possible that, at $q \leq 1.0$, they are higher than 80 °C, the maximum temperature investigated by us, and therefore escape detection. Moreover, as our aforementioned (see Section 3.1) cmc measurements of pure DHPC indicate, no temperature dependence on aggregate structure is expected as $q \rightarrow 0$.

Table 1
Transition temperatures for DMPC/DHPC mixtures heated from 14 to 80 °C

c_L (%)	q	T_{fv} (°C)	T_{ct} (°C)	ΔT_v (°C)
1.0	1.0	na[a]	40	na
1.0	2.0	na[a]	25	na
1.0	3.0	na[b]	ns	na
1.0	4.0	na[b]	ns	na
2.0	1.0	na[c]	80	0
2.0	2.0	28	32	4
2.0	3.0	24	24	1
2.0	4.0	na[c]	24	0
3.0	1.0	na[d]	na[d]	na
3.0	2.0	29	40	10
3.0	3.0	23	25	4
3.0	4.0	na[c]	23	0
5.0	1.0	na[d]	na[d]	na
5.0	2.0	34	46	16
5.0	3.0	24	28	5
5.0	4.0	23	25	4

T_{fv} is the temperature where the initially fluid sample (all samples are fluid as water below 24 °C) becomes viscous. T_{ct} is the temperature where sample turbidity sets on (turbidity is accompanied by a decrease in viscosity for the viscous samples). ΔT_v is the temperature span over which the sample is viscous. "na" = not applicable (the viscous or turbid phase does not exist within the temperature range); "ns" = nonsoluble (turbid at all temperatures).

[a] At low c_L a viscosity increase is expected to be small and could therefore escape our detection.

[b] The sample composition is not soluble, so no viscous phase can appear.

[c] The sample goes directly to a fluid and turbid state, so a viscous phase never appears. This is denoted $\Delta T_v = 0$, i.e., the viscous phase has zero temperature span.

[d] The sample stays in the clear and fluid state up to $T = 80$ °C. The transition temperatures may be higher than this.

3.3. Cryo-TEM investigations

Cryo-TEM pictures were taken in order to investigate in detail the sample morphology at various points in the three dimensions c_L, q and T.

3.3.1. q dependence

Fig. 3 shows a series of cryo-TEM pictures at $c_L = 3.0\%$ and $T = 25$ °C, where q is gradually increased from 2.0 to 4.0.

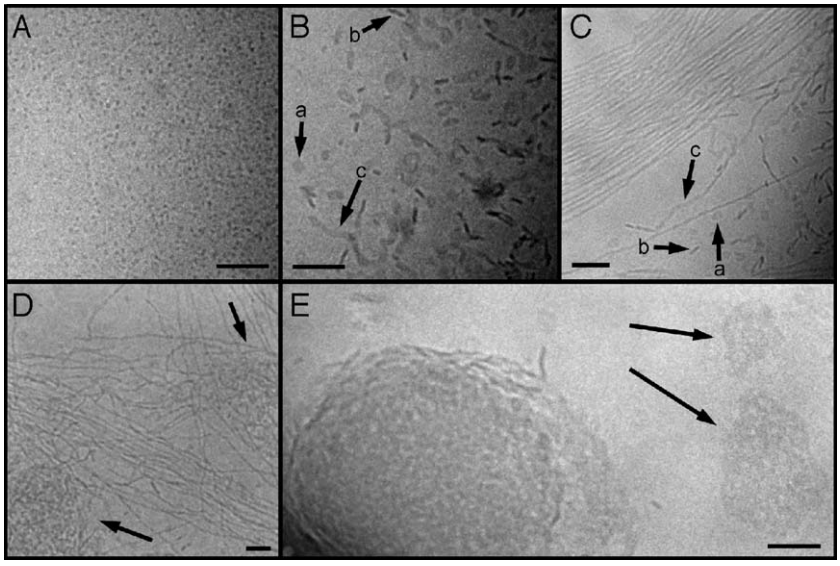

Fig. 3. Cryo-TEM images of aggregates formed by DMPC/DHPC mixtures at 25 °C and $c_L = 3\%$ for $q = 2.0$ (A), $q = 2.2$ (B), $q = 2.5$ (C), $q = 3.0$ (D) and $q = 4.0$ (E). Arrows in B and C point to discs face-on (arrows a) and edge-on (arrows b). Arrow c in B points to elongated distorted discs, and arrow c in C points to a (quasi-)cylindrical micelle where variations in cylinder width are evident. Arrows in D point to large and dense aggregates of branched and entangled (quasi-) cylindrical micelles. Arrows in E point to isolated bilayers which are perforated. Bar = 100 nm in all images (note the different scales).

At $q = 2.0$, Fig. 3A, the sample is dominated by roughly spherical particles that closely resemble globular micelles. At this temperature the sample is clear and has the fluidity of water (see Table 1). Measurements of the aggregate size in the image reveal an aggregate diameter of 7.6 nm (standard deviation 1.7 nm, 100 aggregates measured), suggesting the aggregates to be small discoidal or cylindrical micelles (a mixed globular micelle is expected to have a diameter of roughly 4 nm). However, measurements of these small aggregates are subject to large error due to the influence of the slight under-focus used (which is needed to increase the contrast) as well as the limited digital resolution (the pixel size is 1.6×1.6 nm at the magnification used). A reasonable estimate on the error limit is two pixels, i.e., ~ 3 nm in this case. Therefore, Fig. 3A could depict either globular mixed micelles, small discoidal micelles or short cylindrical micelles, or a mixture of these aggregate types.

As q is increased to 2.2, the sample morphology changes markedly; see Fig. 3B. Roughly disc-shaped aggregates are abundant, though most of them appear to have a somewhat distorted shape (i.e. deviate from a perfectly discoidal shape). The arrows in Fig. 3B point to discs that lie with their normal parallel (“face-on”, arrow a) and perpendicular (“edge-on”, arrow b) to the plane normal. Due to the larger amount of phospholipid material in the way of the electron beam, edge-on discs give a higher contrast against the background (arrow b) as compared to face-on discs (arrow a). Measurements of the size of the more well-shaped discs give a diameter of 23 ± 3 nm (30 aggregates measured). Apart from discoidal structures, many elongated aggregates are also observed (arrow c). They seem to be stretched-out or fused discs, or short flattened cylindrical micelles.

A very dramatic change in sample morphology takes place as q reaches 2.5; see Fig. 3C. At this composition, the sample is viscous but optically clear. Cryo-TEM reveals that the dominant aggregates are very long (several μm) cylindrical micelles. The cylinders appear to be somewhat flattened (arrow c), as observed by the correlated variations in contrast and width along the micelle long axis. This observation, on which we shall elaborate more when discussing the temperature-dependent observations below, means that the cylindrical micelles have a cross-section that deviates somewhat from perfectly circular. Similar flattened cylindrical micelles have been seen in other systems [38]. Noteworthy, these (quasi-)cylindrical micelles coexist with a small population of discs (arrows a (face-on) and b (edge-on)).

As q is further increased the sample starts to become turbid whereupon the viscosity begins to drop. A cryo-TEM picture of a $q = 3.0$ sample is shown in Fig. 3D, where the (quasi-)cylindrical micelles are seen to aggregate into large (>μm) clusters. The outer edges of two such clusters are indicated by the arrows in the figure. These clusters most likely constitute the origin of the sample turbidity. The aggregation also explains the decrease in sample viscosity, since material is effectively being forced out of the solution and into the aggregates. Although not clearly visible in Fig. 3D, we suggest that the clustering occurs due to the formation of branched cylindrical micelles (compare also Fig. 4E). Extensive branching would create a dense interconnected network that loses some of its swelling abilities as compared to the individual cylindrical micelles at $q = 2.5$ (above).

At the highest value of q investigated, $q = 4.0$, the sample viscosity has dropped back to that of water, but the sample

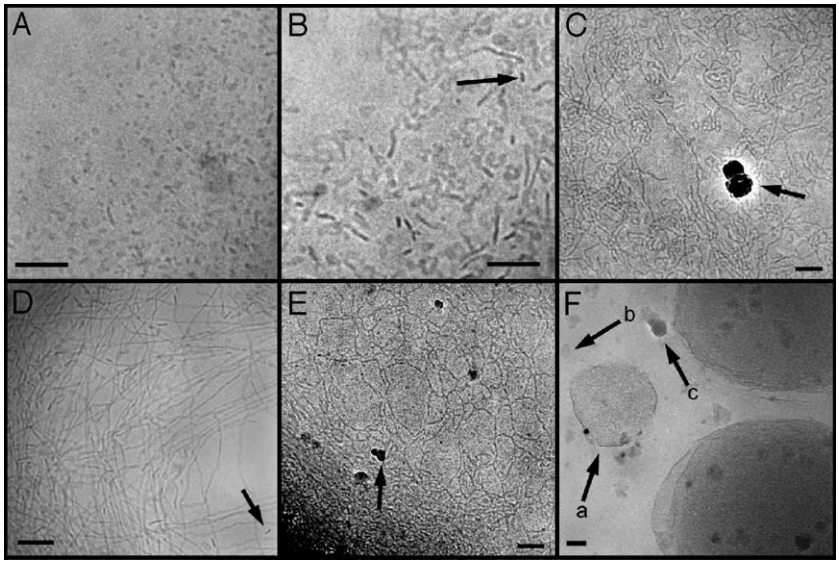

Fig. 4. Cryo-TEM images of aggregates formed by DMPC/DHPC mixtures at $c_L = 3\%$ for $q = 2.0$ at $T = 28$ °C (A), 34 °C (B), 46 °C (C), and for $q = 3.0$ at $T = 24$ °C (D), 34 °C (E) and 40 °C (F). The sample depicted in F was extruded five times through $\phi = 200$-nm filters at 45 °C (see text). Arrows in B and D show discoidal micelles edge-on. Arrows in C and E show ice crystals. Arrows in F show a perforated bilayer that has closed up into a unilamellar vesicle (arrow a), as well as ice crystals of different appearance (arrows b and c). Bar = 100 nm in all images (note the different scales).

is substantially turbid. Fig. 3E shows the aggregate structure in this sample. The aggregates seen in the micrograph are up to micrometers across, and seem to be made up of bilayers, the structure of which appears to be perforated (as indicated by the varying contrast of the bilayer surface seen in the cryo-TEM picture). Similar perforated bilayers have previously been observed in systems containing phosphatidylcholines and conventional surfactants such as SDS and CTAC [39,40]. The arrows in the figure show two individual bilayers of this kind, while the larger aggregate to the lower left in the figure presumably displays a super-structure of several such bilayers stacked on top of each other, where some bilayer fragments at the edge of the super-structure appear edge-on.

3.3.2. Temperature dependence

In Fig. 4, cryo-TEM pictures of two samples, $q = 2.0$ (top row, figures A–C) and $q = 3.0$ (bottom row, figures D–F), both at $c_L = 3\%$, are displayed as a function of temperature. The transitions with increasing temperature are similar to those observed with increasing q-ratio (Fig. 3).

At 28 °C, see Fig. 4A, the $q = 2.0$ sample shows small discoidal aggregates, many of them distorted in shape. The aggregates are obviously different from those observed at 25 °C (shown in Fig. 3A). At a temperature of 34 °C, the $q = 2.0$ sample consists of mainly of cylindrical micelles, although some discs also appear, most of them distorted in shape (see Fig. 4B). The cylindrical micelles are fairly short and appear somewhat flattened, as observed also in the q-dependent study above (Fig. 3C). At this temperature (34 °C) the $q = 2.0$ sample is macroscopically somewhat viscous, although less so than the $q = 2.5–3.0$ samples at 25 °C (where the very long cylinders are observed). The well-shaped discs that remain at 34 °C have a diameter of 20 ± 5 nm (50 aggregates measured). At $T = 46$ °C, the $q = 2.0$ sample is slightly turbid, and has regained the viscosity of water. A cryo-TEM picture of this sample is shown in Fig. 4C, and reveals that the sample contains interconnected thread-like micelles, a similar structure to that observed for the $q = 3.0$ sample at 25 °C (Fig. 3D).

The temperature behavior of the $q = 3.0$ sample, displayed in the bottom row of Fig. 4, shows the domination of very long (quasi-)cylindrical micelles at 24 °C, see Fig. 4D. At this temperature, the sample is highly viscous, almost gel-like. Some aggregation of the quasi-cylinders was observed, although not to the same extent as at the only slightly higher temperature of 25 °C (displayed in Fig. 3D). A few smaller aggregates that may well be discs are also seen (indicated by the arrow). At 34 °C, the sample has become turbid and less viscous, and Fig. 4E shows that at this temperature the flattened cylinders have become highly interconnected. Many cross junctions are seen, leading to a dense aggregate structure. At a higher temperature of 40 °C, the sample turbidity is very high, and the viscosity approximately that of water. The high turbidity indicates that very large aggregates are formed. Due to the technique used for sample preparation [27], aggregates with dimensions larger than about 1 μm (in all dimensions) are excluded from the micrographs. In order to get a representative image of the sample morphology, the sample was therefore extruded five times through 200-nm filters at 40–45 °C. Fig. 4F shows a cryo-TEM image of this extruded sample at 40 °C. The large (≥ 500 nm) aggregates are clearly lamellar, and appear to be perforated (similar to the aggregates depicted in Fig. 3E). In the aggregate pointed at by arrow a, it is evident that the outer edges occasionally appear darker in

the image. It is therefore reasonable to believe that the aggregate is in fact close to a perforated unilamellar vesicle. The same darkened edges are seen also in the two larger aggregates to the right in the figure, and the concentric appearance of the darkened edges of these multi-layered structures indicates that they may be better described as multi-lamellar liposomes. It should be pointed out that the extrusion process itself is likely to contribute to, if not even cause, the closing up of lamellar sheets into vesicles. However, the non-extruded sample at $q=4.0$ displayed in Fig. 3E shows a very similar aggregate structure, indicating that the formation of self-enclosed lamellar structures may also occur spontaneously.

3.3.3. Discs below the DMPC main transition temperature

The results presented above indicate that for $q>2.5$ no pure dispersion of discoidal aggregates exists above the DMPC main transition temperature ($T_m=24$ °C). Most of the samples presented in Table 1 are, however, optically clear and fluid as water below the DMPC main transition temperature. We may thus suspect that also for $q>2.5$ compositions discoidal aggregates can be formed, provided the DMPC bilayer is in a gel phase.

Fig. 5 shows a cryo-TEM micrograph of a $c_L=3\%$ $q=6$ sample at ~20 °C, where the sample is optically clear. Discs are clearly seen throughout the sample, but their average diameter is only 20 nm (±3 nm, 50 discs measured). This is the same size as that of the discs above the DMPC main transition temperature when the disc phase is about to collapse (see Fig. 3B). Apart from discs, bilayer fragments, or sheets, are seen to be abundant in Fig. 5. The sheets have a fairly small area and do not appear to be stacked to a high degree. It seems likely that the sheets are composed of mainly DMPC, which explains the possibility of small discs despite the high sample content of DMPC. Interestingly, the DMPC sheets appear striped in the cryo-TEM image, possibly indicating that DMPC is in the ripple-phase (commonly denoted P'_β; see, e.g., Ref. [31]) rather than in the gel-phase (L_β).

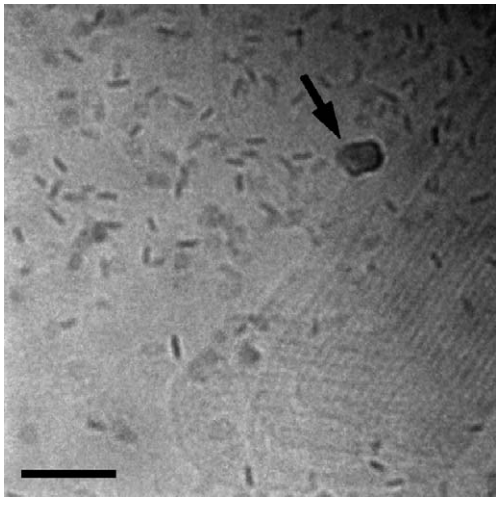

Fig. 5. Cryo-TEM image of a $c_L=3\%$ $q=6.0$ sample at 20 °C displaying discoidal micelles as well as lamellar sheets appearing to be in the ripple phase (see text). Bar = 100 nm.

3.4. Salt dependence

In the literature on DMPC/DHPC bicelles, salt effects have occasionally been observed [19], and low (1:1) salt is often prescribed in the preparative schemes for bicelles. Since the phosphatidylcholine head group is zwitterionic, there should be no sensitivity towards salt concentration on a direct polyelectrolyte level. However, dissolved salts may have the effect of altering the activity of the solute, giving rise to the salting-out phenomenon [41,42]. This has been observed for DHPC micelles with a variety of inorganic salts, amongst them NaCl, where a decrease of the critical micelle concentration was found with increasing [NaCl] [34]. Within the biological range of 0–200 mM NaCl, the effect on DHPC cmc is <2 mM based on the data of Tausk et al. [34], and it is hard to understand the reasons for DMPC/DHPC salt sensitivity on basis of this rather small effect.

In order to investigate the matter of a possible salt dependence, we prepared some samples identical to those in our original (150 mM NaCl) sample-grid above, but without added NaCl (9 mM Na^+ came from adjusting the HEPES buffer to pH 7.4, and another 1.5 mM Na^+ from the added NaN_3). We found no differences in the macroscopically observable phase transitions (viscosity and turbidity) of these salt-free samples as compared to the samples prepared with 150 mM NaCl. There seems, thus, to be no salt dependence in the range studied, at least not detectable by this (admittedly crude) method.

3.5. Disc size by DLS

DLS constitutes a convenient method for analyzing particle size through the dependence of the diffusion coefficient on the particle hydrodynamic radius. A prerequisite for the correct extraction of the hydrodynamic radius is that the diffusion coefficient is measured in the absence of any interparticle interactions. The most straightforward way of ascertaining this is by measuring the diffusion coefficient as function of particle concentration, to make sure there is no concentration dependence (see Eq. (2)). In the present case, however, we may expect a concentration dependence of the particle size, since the population of monomeric DHPC, $[DHPC]_{free}$, presumably does not change upon dilution, and therefore the ratio $q_{eff}=[DMPC]/[DHPC]_{bound}$ will change (see Eq. (6)). Thus it becomes hard to interpret the results from DLS data at low concentration. At $[DHPC]_{bound} \gg [DHPC]_{free}$, it may be possible to find a region of non concentration dependence, but as the total phospholipid concentration c_L increases so will the frequency of interparticle interaction (Eq. (2) is only valid in the limit of low concentration).

We must thus be cautious when interpreting the results from our measurements, and in order to make a distinction between the true hydrodynamic radius, as given by Eq. (3), and the measured quantity through DLS, we introduce the pseudo-hydrodynamic radius R_h':

$$R_h' = \frac{k_B T}{6\pi\eta D} \quad (9)$$

Fig. 6 shows R_h' as a function of total phospholipid concentration, c_L, when a sample at a given q is diluted at 25, 30 and 37 °C. The values of q were limited to $q \leq 1.5$, in order to avoid complications from the increased viscosity as the transition to the cylindrical micellar phase is approached. In the absence of interparticle interactions, i.e., at infinite dilution where $D = D_0$, R_h' is identified as the particle hydrodynamic radius R_h (see Eq. (3)). This condition is plausibly valid for the $q = 0.5$ samples at $\sim 1.5 \leq c_L \leq 3\%$ at the three temperatures investigated, since the concentration dependence becomes negligible in this region (see Fig. 6). The hydrodynamic radius of these aggregates at $c_L = 3.0\%$ reads 3.1–3.2 nm, and is virtually insensitive to temperature in the region examined. For the $q = 1.0$ samples, there is no region of non-concentration dependence, but as c_L approaches 5%, the concentration dependence becomes increasingly less pronounced. At $c_L = 5\%$, the concentration dependence is small, and we believe therefore that the values of R_h' at $c_L = 5.0\%$ are close to the true hydrodynamic radii of the $q = 1.0$ aggregates at all three temperatures investigated (keeping in mind that they may be slightly overstated). The numbers read 3.9, 4.7 and 5.9 nm at $T = 25$, 30 and 37 °C, respectively, and a temperature dependence is thus evident. Also at $q = 1.5$ a temperature dependence of the aggregate diffusion coefficient is clearly borne out, and it seems that it is more pronounced than at $q = 1.0$. There is no region where there is no concentration dependence of the diffusion coefficient, but for $q = 1.5$ at 25 °C we may use the value at $c_L = 5\%$, which reads 6.9 nm, as an upper estimate of the actual hydrodynamic radius. By virtue of Eq. (9), it is seen that a possible small increase in sample viscosity could only decrease the extracted R_h'.

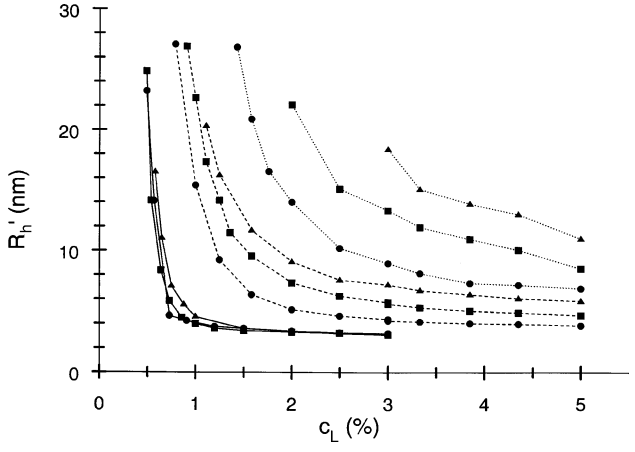

Fig. 6. Pseudo-hydrodynamic radius R_h' (nm) (see text) as function of total phospholipid concentration c_L at $T = 25$ °C (circles), $T = 30$ °C (squares) and $T = 37$ °C (triangles) for $q = 0.5$ (unbroken lines), $q = 1.0$ (broken lines) and $q = 1.5$ (dotted lines). Lines connecting experimental points are to guide the eye.

All curves in Fig. 6 show the same general trend of decreased diffusion coefficient, i.e., increased R_h', with decreasing c_L. Although it is hard, due to the aforementioned reasons, to quantify this behavior, we may safely say that this behavior is due to an increase in aggregate size as the total concentration c_L is lowered, in accordance with Eqs. (6) and (8). For the $q = 0.5$ sample at the two lower temperatures, $T = 25$ and 30 °C, the increase in aggregate size is abrupt, while it is more smooth at $T = 37$ °C. In general, the behavior seems to be smoothened by increased q and elevated temperature. As the size of the aggregates increases, also the polydispersity increases, rendering the interpretation of the DLS measurements increasingly difficult. At $R_h' \approx 20$–25 nm, all the samples start to show turbidity, and it is very interesting that this happens at roughly the same value of R_h' regardless of q, c_L or temperature. We shall elaborate more on this in the discussion to follow.

The increase in particle size as c_L is lowered is likely to be due to the gradual depletion of DHPC from the aggregates, as predicted by the refined ideal disc model (see Eqs. (6) and (8)). Our results, displayed in Fig. 6, show that, for $q = 0.5$ and $q = 1.0$, the increase in aggregate size is fairly independent of temperature. This shows that $[DHPC]_{free}$ is not very temperature-dependent in this temperature range (25–37 °C), in line with the temperature-independent cmc of DHPC reported above. Extrapolation of the curves at $q = 0.5$ and $q = 1.0$ points to $[DHPC]_{free} \approx 5$ mM, independent of q. This result on $[DHPC]_{free}$ is in fair agreement with that found by other investigators [19,37,43].

Our DLS results regarding the aggregate size at $c_L = 3.0\%$ (for $q = 0.5$) and $c_L = 5.0\%$ (for $q = 1.0$ and 1.5) at 25 °C agree well with those of Glover et al. [20], which were measured at $c_L = 10\%$ and 10 °C. At $c_L = 2.5\%$, however, our results deviate significantly from those of Glover et al. [20]. This is likely due to the different temperatures used, and it is noteworthy that these authors have performed their measurements far below the DMPC main transition temperature.

4. Discussion

The findings presented in Results show that small alterations of temperature or sample composition may induce considerable changes in the macroscopic properties of the DMPC/DHPC dispersions. Especially noteworthy are the distinct variations in viscosity and turbidity observed as a function of temperature and/or DMPC/DHPC molar ratio q (Table 1). The results of the cryo-TEM investigations

provide an explanation on the aggregate level for these changes. From the micrographs presented in Figs. 3 and 4, it is clear that the abrupt increase in viscosity is caused by the formation of long (quasi-)cylindrical micelles. Strictly, these extended micelles belong, like the discoidal and globular micelles, to the one-phase region normally termed L_1 (see, e.g., Ref. [44]). However, in order to simplify the terminology, we will refer to the *viscous phase* when discussing the region of the L_1-phase where cylindrical micelles dominate the aggregate structure. Our cryo-TEM results reveal, furthermore, that the macroscopic change from a clear to a turbid dispersion is associated with the formation of dense networks of interconnected (quasi-)cylindrical micelles. Due to the limited swelling ability of these three-dimensional networks, the dispersion develops a tendency to phase-separate. The branched and highly interconnected cylindrical micelles may also be viewed as a transition structure existing just prior to the emergence of the lamellar phase. Based on the available experimental methods, i.e., cryo-TEM and ocular inspections, it is not possible to accurately determine at what composition the lamellar phase actually begins to form. For this reason, we will in the following include both the micellar networks and the aggregates of lamellar structure in what we call the *turbid phase.*

4.1. Phase diagram

From the observations reported above and in Table 1, a three-dimensional "phase"-diagram may be constructed. This phase-diagram, which to our knowledge is the first one published on the DMPC/DHPC system as a function of c_L, q and temperature simultaneously, is shown in Fig. 7. In this plot, which has DHPC and DMPC concentrations on the axes, constant q-values become straight lines of positive slope, and constant c_L-values become straight lines of negative slope. Constant q-lines for $q = 5$, 4, 3, 2, 1 and 0.5 as well as constant c_L-lines for $c_L = 1\%$, 2%, 3% and 5% have been drawn into the phase-diagram for guidance.

The other lines in the phase diagram of Fig. 7 represent phase transition "isotherms" for $T = 24$, 30, 40 and 50 °C, i.e., the sample compositions that produce a phase transition at these temperatures (see figure legend for details). The lines are least-square fits to the data points shown in the figure (see figure legend), which in turn have been extracted from the T_{fv} and T_{ct} data in Table 1, assuming a smooth behavior of the transition temperatures as function of q. Broken lines represent the transition from a clear and fluid to a clear and viscous sample appearance ("T_{fv} isotherms"), indicative of the formation of long (quasi-)cylindrical micelles. Unbroken lines represent the transition from a clear to a turbid phase ("T_{ct} isotherms"), indicating formation of large aggregates. The area between the two isotherms at a given temperature has been shaded, and thus represents DMPC/DHPC compositions that give an optically clear and viscous sample appearance at 24, 30, 40 and 50 °C, respectively.

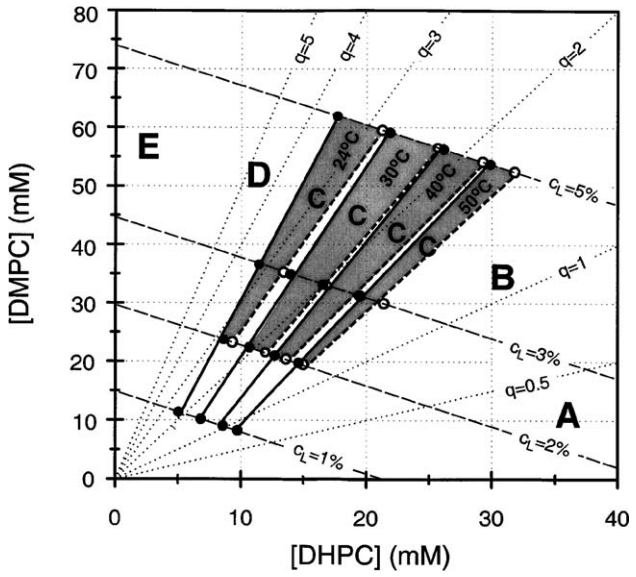

Fig. 7. Phase diagram for the DMPC/DHPC mixtures. Reference lines for q=[DMPC]/[DHPC] = 5.0, 4.0, 3.0, 2.0, 1.0, and 0.5 (dotted), as well as for c_L={m(DHPC) + m(DMPC)}/m(buffer) = 5%, 3%, 2% and 1% (broken) have been drawn. Broken bold lines represent transition "isotherms" for 24, 30, 40 and 50 °C for a macroscopic phase transition from fluid to viscous samples (T_{fv} isotherms). Unbroken bold lines represent transition "isotherms" for 24, 30, 40 and 50 °C where the sample composition is such that a transition occurs from a clear to a turbid sample appearance (T_{ct} isotherms). The lines are least-square fits to data points (open circles for the fluid to viscous transition; filled circles for the clear to turbid transition) extracted from the data presented in Table 1 (T_{fv} and T_{ct}, respectively; see text for details). Shaded areas tie the isotherms together at 24, 30, 40 and 50 °C, respectively, and thus represent the sample compositions that are clear and viscous.

$T = 24$ °C is the DMPC main transition temperature, and below this temperature DMPC is in a gel phase. A lowering of the main transition temperature of DMPC may be expected upon incorporation of DHPC into the bilayer. However, in the discoidal micelles as well as in the perforated lamellar sheets, large domains of virtually pure DMPC are believed to occur, and thus the properties of DMPC should be retained locally. The behavior is therefore expected to be different for DMPC/DHPC mixtures above and below the DMPC main transition temperature. Experimentally it was found that many of our samples went through dramatic changes in terms of turbidity and/or viscosity just at 24 °C (see Table 1). For use as membrane-mimics in the pursuit of biologically relevant biomolecular structures, it is a necessity that the phospholipids are in a liquid crystalline state.

Extrapolation of the two isothermal lines, T_{fv} and T_{ct}, to [DMPC] = 0 gives an estimate of $[DHPC]_{free}$ at the transition from region B to C and region C to D, respectively. At the three temperatures, 30, 40 and 50 °C, the two lines coincide at the x-axis and indicate $[DHPC]_{free}$ values of 4, 5 and 6 mM, respectively. These DHPC concentrations are similar to the concentration extracted from our DLS measurements (see Section 3.5), $[DHPC]_{free} \approx 5$ mM, and to

those found by others [19,37,43]. The fact that the T_{fv} and T_{ct} isotherms cross at [DMPC] ≈ 0 suggests that the concentration of monomeric DHPC remains constant in region C. The slight increase in $[DHPC]_{free}$ with increasing temperature indicates, moreover, that the intrinsic properties of the aggregates change somewhat with temperature. The crudeness of the experimental methods used to determine the data points prevents us, however, from drawing any firm conclusions concerning this possibility and its implications. The isotherms at 24 °C do not coincide at [DMPC] ≈ 0, suggesting different $[DHPC]_{free}$ for the fluid-viscous and the clear-turbid transitions. The gel to liquid crystalline transition of DMPC, which occurs at this temperature, is likely, however, to affect the behavior, rendering the interpretation difficult.

It is clearly seen in the phase-diagram of Fig. 7 that the transition temperatures for both the fluid–viscous and the clear–turbid transitions increase dramatically with decreasing value of q. As long as $[DHPC]_{tot} \gg [DHPC]_{free}$, they appear, however, only to be slightly affected by the value of c_L. This behavior is in agreement with dilution experiments at $q = 2.5$ made by Sanders and Schwonek [11], and with the general trend as function of q found by Raffard et al. [22]. Furthermore, it is interesting that the isotherms at 30, 40 and 50 °C for the transition from discoidal to cylindrical micelles (the transition to the viscous phase, i.e., the T_{fv} isotherms) run roughly parallel to each other, at a slope, d[DMPC]/d[DHPC], of 2.0–2.6. If interpreted within the ideal bicelle model, where $q_{eff} = [DMPC]/[DHPC]_{bound}$ directly controls the disc size (see Eq. (8)), this behavior indicates that the discs collapse into cylinders when they have reached a certain size. q_{eff} is given by the slope of the isotherms, and according to Eq. (8) the maximum diameter is thus 21–26 nm (using $k = 0.6$) or 31–39 nm (using $k = 1.0$). We note that the former theoretical values are fairly well in line with the disc sizes we measure in our cryo-TEM micrographs as the discoidal phase is on the edge of collapsing into the quasi-cylindrical phase (see Figs. 3B and 4B). However, the agreement with theory found at $q \geq 2.0$ may well be coincidal, since we cannot be sure on the DMPC/DHPC composition in the discs in the presence of other aggregates. Whatever the case, it seems that no matter how c_L, q or temperature are manipulated, discs with a larger diameter than ~ 20 nm cannot be produced by the DMPC/DHPC system under present conditions.

It is reassuring that also the DLS data indicate a maximum possible disc size (see Fig. 6). It seems reasonable to argue, although the R_h' measured is not the true hydrodynamic radius, that the disc phase collapses into other (larger) structures when the discs have reached a certain size. The derivation of this result rests on assuming that the sample morphologies of the samples are the same, which is not implausible considering the fairly small variation in q and c_L. Thus, although we are not able to measure the actual size of the aggregates at low c_L using DLS, we believe that our DLS results support the idea of a maximum possible size for the discoidal micelles. Also at temperatures below the DMPC main transition temperature, at the high q-value of 6, a disc diameter of ~ 20 nm is found (see Fig. 5), indicating that the behavior is not restricted to DMPC being in the liquid crystalline phase.

We may, for the purpose of convenient reference in the discussion to come, divide the phase-diagram of Fig. 7 into the five regions, A–E. In region A, as $q \to 0$, the dominating structure is expected to be the mixed globular, or slightly ellipsoidal [35,45], micelle at all temperatures. In region B, at roughly equal amounts of DHPC and DMPC ($q \approx 1$), discoidal micelles may be formed at biological temperature, and this is the interesting region for NMR work on membrane proteins. Region C (shaded areas in the phase diagram) represents the optically clear and viscous phase where long (quasi-)cylindrical micelles are the dominating aggregate structure. At a certain, temperature-dependent, value of q, the samples finally enter region D, the turbid phase. In this region interconnected cylindrical micelles and eventually (at higher q or T) fragments of a holey lamellar phase are found. The onset of turbidity is accompanied by a decrease in viscosity, and this is the region where the magnetically alignable aggregates may form [37]. Region E, finally, represents the part of the phase diagram where the amount of DHPC is too low to disrupt the lamellar phase that DMPC adapts when being the only component.

It should be clear from our results and from the phase diagram in Fig. 7 that manipulation of both temperature and the ratio q leads to the same sequence of aggregate structures, i.e., increasing the temperature is equivalent to decreasing the relative amount of DHPC (or increasing the relative amount of DMPC). This effect could, in principle, be explained by a temperature-dependent concentration of monomeric DHPC. The results reported in Fig. 2 show, however, that the cmc, and thus the aqueous monomer solubility of DHPC, is virtually insensitive to temperature (at least in the temperature range of relevance for the present study). The temperature-induced morphological changes in the DMPC/DHPC system are thus not triggered by an increase in the $[DHPC]_{free}$ per se. Instead the structural transformations appear to be induced by temperature-dependent alterations on the molecular level that lead to a preference for aggregates with decreasing average curvature. One important factor may be the decrease in effective length of the lipid hydrocarbon chains obtained as the degree of *trans-gauche* isomerization increases with temperature [46]. These temperature-dependent alterations may, in turn, give rise to changes in $[DHPC]_{free}$ with temperature, as indicated by extrapolation of the isotherms in the phase-diagram of Fig. 7 (as discussed above).

4.1.1. Region A and B—small aggregates

At $q = 0$, DHPC is the only phospholipid present in the solution, and the aggregates formed by pure DHPC are micelles that are believed to be slightly ellipsoidal [35,45]. DLS measurements on a 50 mM DHPC solution (20 mM

HEPES, pH 7.4, 150 mM NaCl, $T=25$ °C) show the hydrodynamic radius of the DHPC micelles to be 1.9 nm (data not shown). Using the relation $l_{max}=0.1265\times(n_c-1)+0.15$ for the maximum length of the fatty acid chain [47] (l_{max} in nm), with n_c the number of carbons ($n_c=6$ for DHPC), and a phosphatidylcholine head group thickness of 0.9 nm [31], an estimate of the (all-*trans*) DHPC molecular length reads ~1.7 nm. Our DLS measurements thus point to a DHPC micellar shape that is close to, but not quite, globular. A more accurate determination of the micellar shape is beyond the scope of the present investigation.

At $q=0.5$, DLS shows the hydrodynamic radius of the existing DMPC/DHPC aggregates to be about 3.1 nm (see Fig. 6). If interpreted as a globular micelle, this hydrodynamic radius corresponds to a sphere of radius 3.1 nm. The DMPC hydrocarbon chain is 1.0 nm longer (the projected length in the all-*trans* carbon chain direction, see the relation above) than that of DHPC if both are maximally extended, and so the differences in radii between the $q=0.5$ and the $q=0$ aggregates may almost be accounted for by differences in hydrocarbon chain length. It seems reasonable that at sufficiently low values of q, the small amount of DMPC is simply incorporated into the DHPC-dominated micelle. However, as q increases, also the hydrodynamic radius of the DMPC/DHPC aggregates is substantially increased, as clearly seen in Fig. 6. This is not consistent with what is expected for globular micelles, which cannot have a radius larger than the length of the molecules that form them. Some other aggregate must be formed already at, or just above, q values of 0.5. Glover et al. [20] report similar results on the DMPC/DHPC aggregate radius from DLS measurements at low q-values and 10 °C, and show that aggregates with $R_h'>4$ nm are well described as having a discoidal shape.

If our DLS results from the $q=0.5$ sample are interpreted as a disc, Eq. (4) yields a disc radius of $r'=3.1$ nm (see Fig. 1 for notation). Subtracting the rim radius, $r\approx 2$ nm [4], leaves a disc center radius of merely $R=1.1$ nm, corresponding to a bilayer area of 3.7 nm^2 on every side of the disc. With a head group area of 0.60 nm^2 for DMPC in a bilayer environment [31], this area corresponds to about six DMPC molecules on each side of the bilayer. It is doubtful if one can speak of a disc at all in this case. In fact, it appears questionable whether it is meaningful to try to distinguish between different shapes of aggregates barely larger than the size of a globular micelle. The rather small size of the discs at $q=0.5$ constitutes an important observation, since $q=0.5$ is commonly used in membrane–protein (peptide) structural elucidation by NMR spectroscopists [5,7,48].

The ideal disc model gives a disc radius of 6.1 nm for $q=0.5$, i.e., roughly double that found experimentally. Invoking the refined ideal disc model, see Eqs. (6) and (8), the expected radius becomes 6.6 nm when using $[DHPC]_{free}=5$ mM, $c_L=3\%$ and $k=1$. Using the same values for $[DHPC]_{free}$ and c_L, but $k=0.6$ instead, the theoretical radius becomes 5.1 nm, which is still larger by far than the radius found experimentally. The predictions of the models at $q=1.0$ give the same sort of deviations. Experimentally a hydrated radius of 3.9 nm is found for the $q=1.0$ sample at 25 °C (at $c_L=5\%$), which may be slightly overstated (see Results). This translates to a disc radius of 4.15 nm through Eq. (4). The ideal disc model gives 9.4 nm, and the refined ideal disc model 7.3 nm (using $[DHPC]_{free}=5$ mM, $c_L=5\%$ and $k=0.6$). Also at $q=1.5$, the predictions are overestimating the experimentally found hydrodynamic radii ($R_h'=6.9$ nm at 25 °C, translating to $r'=8.2$ nm).

Cryo-TEM micrographs at $q=2.0$ ($c_L=3\%$, $T=25$ °C), as displayed in Fig. 3A, show the existence of small apparently homogeneous and symmetric aggregates with a diameter of 6–9 nm, i.e., a disc radius of around 4 nm. Under these conditions, the refined ideal disc model predicts a disc radius of 11.9 nm (using $k=0.6$ and $[DHPC]_{free}=5$ mM), thus again widely overestimating the experimentally found disc size. Cryo-TEM micrographs were also taken of samples at $q=0.5$, 1.0 and 1.5 at 25 °C (data not shown). These show aggregates similar to those depicted in Fig. 3A, with a radius of approximately 3 nm. As remarked upon before, measurements of these small aggregates are very uncertain due to the influence of the under-focus used as well as the limited digital resolution. The results that are in line with those from DLS show, nonetheless, the disc size at $q\leq 2.0$ to be much smaller compared to that predicted by any of the disc models at 25 °C.

There are two immediate ways to adjust the theoretical model to obtain better agreement with experimentally found disc sizes. One is to decrease the k-factor substantially, forcing the conclusion that the head group area of DHPC is substantially larger than that of DMPC. If the value 0.60 nm^2 for the head group area of DMPC in a bilayer arrangement is correct, this would lead to a DHPC head group area of 2–3 nm^2. This seems physically unrealistic as well as contrary to available experimental indications on the head group size in DHPC micelles, i.e., 0.66 nm^2 [34] and 1.02 nm^2 [35]. The other way to adjust the theory is to allow for DMPC to take part in the rim of the disc, in this way making some DMPC behave as if it were DHPC, and thus effectively decreasing the ratio q (or q_{eff}). Although we are not in a position to put forward any rigorous theoretical model, our experimental results can be fairly accurately predicted by assuming that ~60% of the available DMPC goes into the rim of the disc. This result assumes $k=0.6$ for the relative head group areas of the bilayer- and rim-forming constituents, and it should be noted that it is the product of k and q_{eff} that enters into the theoretical expressions (see Eq. (8)). Many combinations of these two factors will thus yield similar results and, furthermore, it is obvious that the DMPC participation in the disc rim could be formulated in more than one way. We suggest, however, that this approach is likely to point in the right

direction, i.e., that vast DMPC participation in the rim occurs, resulting in smaller discs than predicted by the ideal disc models.

4.1.2. Region C—cylindrical micelles

Dramatic morphological changes take place as we move from region B to region C in the phase diagram. Very long (>μm) cylindrical micelles are formed, as is evident in Figs. 3C and 4D. At the same time, the sample viscosity dramatically increases, an effect that has been quantified in Ref. [37] to 2–3 orders of magnitude for $c_L = 3-5\%$. This dramatic increase in viscosity has been noted by several investigators, and recently a gradual disc–lamellar transition [14] and a transitional cubic phase [15] have been put forward as explanations. Cylindrical micelles have, to our knowledge, not been proved or suggested in this system before, however. The presence of these very extended cylindrical micelles gives a straightforward explanation for the high sample viscosity. As seen in the phase-diagram in Fig. 7, the temperature for the onset of the cylindrical micellar phase (as evidenced by a dramatic increase in sample viscosity) is highly q-dependent (broken lines). At $q \approx 3$ and higher, cylindrical micelles form already at the DMPC main transition temperature.

Our cryo-TEM micrographs suggest that the cylindrical aggregates are not perfectly symmetric around their long axis. This is most clearly seen in Fig. 3C, indicated by arrow c, where contrast variations correlated with differences in cylinder width are evident. This is suggestive of a non-circular micellar cross section, and hence we use the term ''quasi-cylindrical'' to describe the shape of these aggregates. The deviation from perfect cylindrical symmetry is, however, modest.

4.1.3. Region D—micellar networks and a holey lamellar phase

As the ratio q or the temperature is further increased in region C in the phase diagram, the long (quasi-)cylindrical micelles start to merge into branched micelles. This is most evident upon comparing Fig. 4D and E, but also evident when comparing Fig. 3C and D. Upon this branching, large networks with limiting swelling ability are formed. Macroscopically this is observed as the onset and subsequent increase of sample turbidity, and a simultaneous decrease in sample viscosity. The temperature-dependent macroscopic phase-separation observed through the turbidity change signifies the entrance into region D of the phase diagram of Fig. 7.

Eventually, as q or temperature is further increased, the network of branched cylindrical micelles transforms into large lamellar aggregates, see Figs. 3E and 4F. At this point, the sample turbidity is substantial, whereas the viscosity has dropped back approximately to that of pure solvent. The drop in viscosity is indicative of entering the region where magnetically alignable DMPC/DHPC aggregates may appear [37]. The sample compositions and temperatures that give rise to a stable liquid crystalline phase in the NMR magnet, according to the extensive study by Ottiger and Bax [19], occur in this region of the phase diagram. Large aggregates like lamellar sheets may well have a magnetic susceptibility anisotropy large enough to orient in magnetic fields [49–51], a property that is questionable for the relatively small discs [37]. It is evident, especially from Fig. 3E, but also from Fig. 4F, that the lamellar sheets are disrupted, as seen by the varying intensity along the plane of the sheet. We suggest therefore that the aggregate structure depicted in Fig. 3E is a lamellar sheet perforated by holes, much like a slice of Swiss cheese.

Considerations of curvature (we return to this below) suggest that DHPC should preferably cover the edges of the holes in the DMPC dominated lamellar sheet. The appearance of two distinct peaks in the ^{31}P-NMR spectrum, with relative intensities (roughly) equal to the DMPC/DHPC ratio q [11,19,22,26,52], supports DHPC and DMPC being separated into different domains under these conditions. Further evidence to this end comes from the absence of ^{1}H NOESY DMPC-DHPC cross-peaks under similar conditions [23]. Therefore, a Swiss-cheese model where DHPC covers the edges of the holes in a DMPC dominated lamellar sheet seems to fit available data well. Such a model has recently been suggested also by others, on basis of NMR probe diffusion experiments [13], fluorescent probe experiments [15] and SANS data [24]. We further suggest the DHPC edged holes to be rather large, since the negative curvature associated with small holes is not in line with the preference of DHPC (since pure DHPC forms close to globular micelles).

4.1.4. Region E—lamellar phase

Fig. 4F, corresponding to a sample with composition $c_L = 3\%$ $q = 3.0$ at $T = 40$ °C, shows large lamellar aggregates that seem to be under way of closing up on themselves, i.e., to form vesicular structures. It should be remembered that this sample has been extruded through 200 nm filters, in order to decrease the particle size. It is likely that this manipulation has the effect of inducing the formation of self-closed structures. The lamellar structures appear to be perforated in a similar fashion as evident in the $c_L = 3\%$ sample at $q = 4.0$ and 25 °C (see Fig. 3E). DMPC forms a lamellar L_α phase in the absence of DHPC, i.e., at $q = \infty$, and it seems logical that DHPC is simply incorporated into the bilayer when present in sufficiently low amounts. Transient pores form spontaneously in the bilayer, and it is plausible that the micellar-forming DHPC molecules have a propensity to adsorb at the edges of these pores [53]. The accumulation of DHPC has a stabilizing effect on the pores, and with increasing DHPC concentration their lifetime increases. The formation of long-lived pores leads from region E (the nonperforated lamellar phase) into region D (the perforated lamellar, or ''Swiss cheese'', phase) of the phase diagram depicted in Fig. 7. The methods at our disposal cannot determine at precisely which compositions

to draw the line between regions D and E, if such a marked line can be defined at all.

4.2. Summary of encountered structures and transitions

Several aggregate structures are seen in the DMPC/DHPC system, and the phase-diagram is quite complex (see Fig. 7). The ratio of the two phospholipid components, q (q=[DMPC]/[DHPC]), and the temperature, T, appear to be the variables that directly affect the sample morphology, while c_L only has a slight effect when $[DHPC]_{tot} \gg [DHPC]_{free}$. Increasing the temperature has the same effect as increasing the ratio q. It is expected that the aggregate curvature decreases with increasing q, since pure DMPC forms an extended lamellar phase of close to zero curvature (see, e.g., Ref. [44]).

Fig. 8 shows the sequence of aggregates observed as function of q and T in cartoon form. At low values of q, roughly globular micelles are formed (the structure of these aggregates may be somewhat ellipsoidal [35,45]). As q increases, or at elevated temperatures, small nonspherical structures, presumably with a discoidal shape [20], are formed. The center is most likely largely made up by DMPC, while the rim is made up of both DMPC and DHPC. The discoidal aggregates grow in size as q or temperature is further increased, but only to a diameter of about 20 nm, whereafter cylindrical micelles start to form. The cylindrical micelles are slightly flattened (‘‘quasi-cylinders’’) and presumably made up of intimately mixed DMPC and DHPC. It seems likely that the rim of the discoidal micelles has roughly the same DMPC/DHPC composition as the first cylindrical micelles formed, rendering the transition smooth. As q or the temperature is further elevated, the cylindrical micelles start to interconnect. Formation of an interconnected network lowers the average curvature of the aggregates due to the decreasing number of ends (which are highly curved) as well as due to the negative curvature at the branching points. Since the curvature is low in the junctions, there may be a gradual enrichment of DMPC at these points. It is straightforward to see how a further increase in q or temperature transforms this structure into a perforated lamellar phase reminiscent of a slice of Swiss cheese. The holes in the lamellar phase, which are presumably edged by DHPC, must be rather large in order to overcome the negative curvature imposed on this ‘‘inverted rim’’.

The intermediate structure of a partly segregated discoidal micelle ‘‘sandwiched’’ between the mixed globular and the mixed cylindrical micelles is somewhat mysterious. A transition directly from mixed globular to mixed cylindrical micelles seems more natural, and such transitions are commonly observed in other surfactant/phospholipid systems (Ref. [39] and references therein). However, small discoidal micelles may be able to better match the preferred curvature of DMPC and DHPC separately, by partly segregating the molecules into the non-curved center and the curved rim of the disc, respectively. This constitutes a situation of relatively low entropy, however, and as the disc grows larger (with increasing q or temperature), the entropic cost of this aggregate structure increases. Furthermore, as the rim of the discs grows larger, their decreasing curvature becomes less attractive for DHPC. In response to this, more DMPC may be directed into the rim, and eventually the formation of only rims, i.e., elongated (quasi-)cylinders, is favoured over discoidal structures. This would explain why the discoidal micelles are limited in size, as observed experimentally.

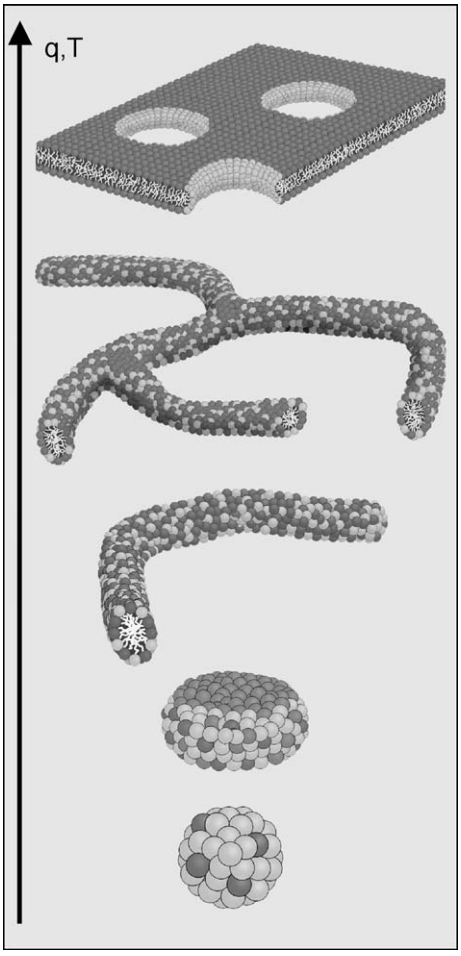

Fig. 8. Cartoon showing the aggregate structures encountered in DMPC/DHPC mixtures as a function of either q or T. From bottom to top: a mixed globular micelle; a discoidal micelle with DMPC in the center and both DMCP and DHPC in the rim; a mixed cylindrical micelle that is slightly flattened (a quasi-cylinder); branched mixed quasi-cylindrical micelles; and a holey DMPC lamellar sheet where DHPC covers the edges of the holes. Black head groups represent DMPC, light-grey head groups represent DHPC.

5. Conclusions

We have investigated DMPC/DHPC aggregate structures and their transitions by means of ocular inspection and cryo-

TEM, and constructed a three-dimensional phase-diagram in the region $1\% \leq c_L \leq 5\%$ and $q \leq 4$ (depicted in Fig. 7). We find that both increasing temperature and increasing the DMPC/DHPC molar ratio q lead to the same sequence of aggregate formation. The total phospholipid concentration c_L has a less pronounced effect on the aggregate structure. The general transformation is from mixed globular micelles, via small discs on to (quasi-)cylindrical micelles which branch and finally turn into a perforated lamellar sheet (see Fig. 8).

By means of DLS, we find that the discs at low q ($q < 1.5$) are significantly smaller than what is predicted by the refined ideal disc model. This could be explained by vast DMPC participation in formation of the rim. $q = 0.5$ discs at $T = 25–37$ °C, the composition typically used as "bicelles" in NMR, have a bilayer area corresponding to approximately six DMPC molecules (on either side). Furthermore, the discs seem to have a maximum diameter of $\sim$ 20 nm. Elevation of the temperature or the DMPC/DHPC ratio q to attain larger discs leads to distorted discs that become lengthened and eventually turn into cylindrical micelles.

The dramatic increase in viscosity at intermediate DMPC/DHPC ratios ($2.0 \leq q \leq 3.5$) is due to the formation of very long cylindrical micelles, which are somewhat flattened (i.e. "quasi-cylindrical"). The structure of this phase may have important implications for the development of bicelle membrane protein crystallization methods, by aiding an understanding of the mechanism. Upon increasing q or temperature, the quasi-cylindrical micelles become branched, and eventually extended perforated lamellar sheets, reminiscent of slices of Swiss cheese, are formed. This is accompanied by a decrease in viscosity, and these aggregates most likely constitute the magnetically alignable DMPC/DHPC mixtures used in solution NMR.

Acknowledgements

We are indebted to Wyn Brown for invaluable expertise in the light-scattering area. Mats Almgren is thanked for helpful discussions. Financial support was obtained from the Swedish Research Council (Vetenskapsrådet) and the Swedish Cancer Society (Cancerfonden).

References

[1] J. Bian, M.F. Roberts, Phase separation in short-chain lecithin/gel-state long-chain lecithin aggregates, Biochemistry 29 (1990) 7928–7935.
[2] D.M. Small, S.A. Penkett, D. Chapman, Studies on simple and mixed bile salt micelles by nuclear magnetic resonance spectroscopy, Biochim. Biophys. Acta 176 (1969) 178–189.
[3] N.A. Mazer, G.B. Benedek, M.C. Carey, Quasielastic light-scattering studies of aqueous biliary lipid systems. Mixed micelle formation in bile salt-lecithin solutions, Biochemistry 19 (1980) 601–615.
[4] R.R. Vold, R.S. Prosser, Magnetically oriented phospholipid bilayered micelles for structural studies of polypeptides. Does the ideal bicelle exist? J. Magn. Reson., B 113 (1996) 267–271.
[5] R.R. Vold, R.S. Prosser, A.J. Deese, Isotropic solutions of phospholipid bicelles: a new membrane mimetic for high-resolution NMR studies of polypeptides, J. Biomol. NMR 9 (1997) 329–335.
[6] C.R. Sanders II, K. Oxenoid, Customizing model membranes and samples for NMR spectroscopic studies of complex membrane proteins, Biochim. Biophys. Acta 1508 (2000) 129–145.
[7] J.A. Whiles, R. Deems, R.R. Vold, E.A. Dennis, Bicelles in structure–function studies of membrane-associated proteins, Bioorg. Chem. 30 (2002) 431–442.
[8] N. Tjandra, A. Bax, Directs measurements of distances and angles in biomolecules by NMR in a dilute liquid crystalline medium, Science 278 (1997) 1111–1114.
[9] J.H. Prestegard, A.I. Kishore, Partial alignment of biomolecules: an aid to NMR characterization, Curr. Opin. Chem. Biol. 5 (2001) 584–590.
[10] A. Bax, Weak alignment offers new NMR opportunities to study protein structure and dynamics, Protein Sci. 12 (2003) 1–16.
[11] C.R. Sanders II, J.P. Schwonek, Characterization of magnetically orientable bilayers in mixtures of dihexanoylphosphatidylcholine and dimyristoylphosphatidylcholine by solid-state NMR, Biochemistry 31 (1992) 8898–8905.
[12] C.R. Sanders II, B.J. Hare, K.P. Howard, J.H. Prestegard, Magnetically oriented phospholipid micelles as a tool for the study of membrane-associated molecules, Prog. NMR Spectroscopy 26 (1994) 421–444.
[13] S. Gaemers, A. Bax, Morphology of three lyotropic liquid crystalline biological NMR media studied by translational diffusion anisotropy, J. Am. Chem. Soc. 123 (2001) 12343–12352.
[14] M.-P. Nieh, C.J. Glinka, S. Krueger, R.S. Prosser, J. Katsaras, SANS study on the effect of lanthanide ions and charged lipids on the morphology of phospholipid mixtures, Biophys. J. 82 (2002) 2487–2498.
[15] B.A. Rowe, S.L. Neal, Fluorescence probe study of bicelle structure as a function of temperature: developing a practical bicelle structure model, Langmuir 19 (2003) 2039–2048.
[16] S. Faham, J.U. Bowie, Bicelle crystallization: a new method for crystallizing membrane proteins yields a monomeric bacteriorhodopsin structure, J. Mol. Biol. 316 (2002) 1–6.
[17] M. Caffrey, Membrane protein crystallization, J. Struct. Biol. 142 (2003) 108–132.
[18] L.A. Holland, A.M. Leigh, Bilayered phospholipid micelles and capillary electrophoresis: a new additive for electrokinetic chromatography, Electrophoresis 24 (2003) 2935–2939.
[19] M. Ottiger, A. Bax, Characterization of magnetically oriented phospholipid micelles for measurement of dipolar couplings in macromolecules, J. Biomol. NMR 12 (1998) 361–372.
[20] K.J. Glover, J.A. Whiles, G. Wu, N. Yu, R. Deems, J.O. Struppe, R.E. Stark, E.A. Komives, R.R. Vold, Structural evaluation of phospholipid bicelles for solution-state studies of membrane-associated biomolecules, Biophys. J. 81 (2001) 2163–2171.
[21] C.R. Sanders II, R.S. Prosser, Bicelles: a model membrane system for all seasons? Structure 6 (1998) 1227–1234.
[22] G. Raffard, S. Steinbruckner, A. Arnold, J.H. Davis, E.J. Dufourc, Temperature–composition diagram of dimyristoylphosphatidylcholine–dicaproylphosphatidylcholine "bicelles" self-orienting in the magnetic field. A solid state ^{2}H and ^{31}P NMR study, Langmuir 16 (2000) 7655–7662.
[23] E. Sternin, D. Nizza, K. Gawrisch, Temperature Dependence of DMPC/DHPC mixing in a bicellar solution and its structural implications, Langmuir 17 (2001) 2610–2616.
[24] M.-P. Nieh, C.J. Glinka, S. Krueger, SANS study of the structural phases of magnetically alignable lanthanide-doped phospholipid mixtures, Langmuir 17 (2001) 2629–2638.
[25] P.A. Luchette, T.N. Vetman, R.S. Prosser, R.E.W. Hancock, M.-P.

Nieh, C.J. Glinka, S. Krueger, J. Katsaras, Morphology of fast tumbling micelles: a small angle neutron scattering and NMR study, Biochim. Biophys. Acta 1513 (2001) 83–94.
[26] A. Arnold, T. Labrot, R. Oda, E.J. Dufourc, Cation modulation of bicelle size and magnetic alignment as revealed by solid-state NMR and electron microscopy, Biophys. J. 83 (2002) 2667–2680.
[27] M. Almgren, K. Edwards, G. Karlsson, Cryo-transmission electron microscopy of liposomes and related structures, Colloids Surf., A 174 (2000) 3–21.
[28] J. Jakes, Testing of the constrained regularization method of inverting Laplace transform on simulated very wide quasielastic light scattering autocorrelation functions, Czechoslov. J. Phys., B 38 (1988) 1305–1316.
[29] T. Nicolai, W. Brown, R.M. Johnsen, P. Stepanek, Dynamic behaviour of Θ solutions of polystyrene investigated by dynamic light scattering, Macromolecules 23 (1990) 1165–1174.
[30] M. Corli, V. Degiorgio, Quasi-elastic light scattering study of intermicellar interactions in aqueous sodium dodecyl sulfate solutions, J. Phys. Chem. 85 (1981) 711–717.
[31] J.F. Nagle, S. Tristam-Nagle, Structure of lipid bilayers, Biochim. Biophys. Acta 1469 (2000) 159–195.
[32] P. Alexandridis, J.F. Holzwarth, T.A. Hatton, Micellization of poly (ethylene oxide)-poly(propylene oxide) triblock copolymers in aqueous solutions: thermodynamics of copolymer association, Macromolecules 27 (1994) 2414–2425.
[33] E.D. Cehelnik, R.B. Cundall, J.R. Lockwood, T.F. Palmer, Solvent and temperature effects on the fluorescence of all-*trans*-1,6-diphenyl-1,3,5.hexatriene, J. Phys. Chem. 79 (1974) 1369–1376.
[34] R.J.M. Tausk, J. Karmiggelt, C. Oudshoorn, J.Th.G. Overbeek, Physical chemical studies of short-chain lecithin homologues. I. Influence of the chain length of the fatty acid ester and of electrolytes on the critical micelle concentration, Biophys. Chemist. 1 (1974) 175–180.
[35] T.-L. Lin, S.-H. Chen, N.E. Gabriel, M.F. Roberts, Use of small-angle neutron scattering to determine the structure of dihexanoylphosphatidylcholine micelles, J. Am. Chem. Soc. 108 (1986) 3499–3507.
[36] R.A. Burns Jr., M.F. Roberts, R. Dluhy, R. Mendelsohn, Monomer-to-micelle transition of dihexanoylphosphatidylcholine: ^{13}C and Raman studies, J. Am. Chem. Soc. 104 (1982) 430–438.
[37] J. Struppe, R.R. Vold, Dilute bicellar solutions for structural NMR work, J. Magn. Reson. 135 (1998) 541–546.
[38] J. Gustafsson, G. Orädd, M. Nyden, P. Hansson, M. Almgren, Defective lamellar phases and micellar polymorphism in mixtures of glycerol monooleate and cetyltrimethylammonium bromide in aqueous solution, Langmuir 14 (1998) 4987–4996.
[39] M. Almgren, Mixed micelles and other structures in the solubilization of bilayer lipid membranes by surfactants, Biochim. Biophys. Acta 1508 (2000) 146–163.
[40] M. Silvander, G. Karlsson, K. Edwards, Vesicle solubilization by alkyl sulfate surfactants: a cryo-TEM study of the vesicle to micelle transition, J. Colloid Interface Sci. 179 (1996) 104–113.
[41] W.F. McDevit, F.A. Long, The activity coefficient of benzene in aqueous salt solutions, J. Am. Chem. Soc. 74 (1952) 1773–1777.
[42] P. Murkerjee, Salt effects on nonionic association colloids, J. Phys. Chem. 69 (1965) 4038–4040.
[43] B.E. Ramirez, O.V. Voloshin, R.D. Camerini-Otero, A. Bax, Solution structure of DinI provides insight into its mode of RecA inactivation, Protein Sci. 9 (2000) 2161–2169.
[44] D.F. Evans, H. Wennerström, The Colloidal Domain—Where Physics, Chemistry, Biology and Technology Meet, VHC Publishers, New York, 1994.
[45] R.J.M. Tausk, J. van Esch, J. Karmiggelt, G. Voordouw, J.Th.G. Overbeek, Physical chemical studies of short-chain lecithin homologues: II. Micellar weights of dihexanoyl- and diheptanoylecithin, Biophys. Chem. 1 (1974) 184–203.
[46] J.N. Israelachvili, Intermolecular and Surface Forces, 2nd ed., Academic Press, San Diego, 1991.
[47] C. Tanford, The Hydrophobic Effect: Formation of Micelles and Biological Membranes, 2nd ed., Krieger Publishing, Malabar, 1991.
[48] A. Andersson, L. Mäler, NMR solution structure and dynamics of motilin in isotropic phospholipid bicellar solution, J. Biol. NMR 24 (2002) 103–112.
[49] J. Seelig, F. Borle, T.A. Cross, Magnetic ordering of phospholipid membranes, Biochim. Biophys. Acta 814 (1985) 195–198.
[50] B.J. Forrest, L.W. Reeves, New lyotropic liquid crystals composed of finite nonspherical micelles, Chem. Rev. 81 (1981) 1–14.
[51] X. Qiu, P.A. Mirau, C. Pidgeon, Magnetically induced orientation of phosphatidylcholine membranes, Biochim. Biophys. Acta 1147 (1993) 59–72.
[52] J.A. Losonczi, J.H. Prestegard, Improved dilute bicelle solutions for high-resolution NMR of biological macromolecules, J. Biomol. NMR 12 (1998) 447–451.
[53] K. Edwards, M. Almgren, Surfactant-induced leakage and structural change of lecithin vesicles: effect of surfactant headgroup size, Langmuir 8 (1992) 824–832.